Fission mode properties from fragment mass distributions

Cédric Simenel[1,2,*] and *Patrick* McGlynn[3,**]

[1]Department of Fundamental and Theoretical Physics, Research School of Physics, Australian National University, Canberra, ACT 2601, Australia
[2]Department of Nuclear Physics and Accelerator Applications, Research School of Physics, Australian National University, Canberra, ACT 2601, Australia
[3]Facility for Rare Isotope Beams, Michigan State University, East Lansing 48824, USA

Abstract. Fission fragment mass distributions often display multiple structures, commonly interpreted in terms of distinct "fission modes." These are usually obtained through multi-Gaussian fits of experimental yields, assuming each Gaussian corresponds to a separate fission channel. However, theoretical models define fission modes in terms of valleys in the potential energy surface (PES) near scission, raising questions about how these "Gaussian modes" relate to the underlying dynamics. We introduce a simple scission-point-inspired model to connect observed yield distributions with effective potentials, providing a means to identify "effective fission modes." Comparisons between Gaussian and effective modes reveal that multiple Gaussian components can correspond to a single underlying fission mode. Analyses of ^{180}Hg and actinide fission show that asymmetric and symmetric modes emerge naturally from the shape of the effective potential and its evolution with excitation energy.

1 Introduction

Fission fragment mass and charge distributions provide a powerful probe of nuclear dynamics. The discovery of asymmetric fission yields led to the introduction of the concept of "fission modes". Fission modes have been studied in various regions of the nuclear chart (see, e.g., [1–3]). These modes are typically linked to shell effects in the fissioning system [4, 5] and in the nascent fragments [6–8].

Similar shell effects are expected to affect heavy-ion reaction mechanisms such as the quasi-fission process that is known to hinder the formation of superheavy elements (see, e.g., [9–11]). Indeed, time-dependent Hartree-Fock (TDHF) calculations predict that quasi-fission and fission can populate the same modes [12–19] (see [20] for a recent review of TDHF applications to nuclear dynamics), although experimental signatures are not as clear [21].

Although Gaussian fits of fragment yields have been remarkably successful in empirical systematics, they lack a one-to-one correspondence with theoretical fission valleys in the potential energy surfaces (PES) [22]. Microscopic models such as the time-dependent generator coordinate method (TDGCM) [23, 24] show that the actual yield shape is rarely Gaussian. The question remains: how do experimental Gaussian components reflect the physical landscape of the fissioning system near scission?

Inspired by the scission point model [6], we extract "effective potentials" from fission fragment mass distributions [22]. These effective potentials could be compared to theoretical potential energy along the scission line extracted from PES, provided the latter are free of discontinuities [25]. Here, we focus on the comparison between Gaussian modes and effective fission modes extracted from the effective potentials.

*e-mail: cedric.simenel@anu.edu.au
**e-mail: mcglynn@frib.msu.edu

2 Theoretical framework

2.1 Mass asymmetry coordinate

We define a unitless mass asymmetry parameter

$$x = 4\frac{A_1 - A_T/2}{A_T}, \tag{1}$$

where A_1 and A_T denote the fragment and compound nucleus masses, respectively. Symmetric fission corresponds to $x = 0$, while $x > 0$ and $x < 0$ represent complementary asymmetric splits.

2.2 Scission-point-inspired yields

Following the scission-point approach [6], we assume a quasi-equilibrium between collective coordinates at scission and write the yield as

$$Y(x) = e^{-V(x)/T}, \tag{2}$$

where $V(x)$ denotes the potential energy along the scission line, and T represents the effective temperature of the system. This allows us to define an "effective potential" from any given yield distribution:

$$V(x) = -T\ln[Y(x)] + \text{const.} \tag{3}$$

This mapping connects the experimentally measured distribution directly to a potential landscape, revealing minima ("effective modes") that may or may not correspond to Gaussian fit centroids.

2.3 Definitions of fission modes

We differentiate between:

- **Gaussian modes**: empirical Gaussian components used to fit data.
- **Theoretical modes**: valleys or minima in the PES derived from microscopic calculations.
- **Effective modes**: minima in the reconstructed $V(x)$ derived from the observed yield.

This distinction is crucial for interpreting fission data in terms of underlying physics rather than empirical fitting.

3 From potential to yield: illustrative examples

To illustrate how Gaussian fits may misrepresent the underlying physical mode, we compute yields for schematic potentials.

3.1 Single-well symmetric potential

For a purely quadratic potential $V \propto x^2$, the yield is exactly Gaussian. For a quartic potential $V = x^4$, however, the yield deviates from Gaussian, and satisfactory fits require multiple Gaussian components as shown in Fig. 1. Multiple Gaussians are needed despite a single underlying mode, showing that overfitting does not necessarily introduce new physical modes.

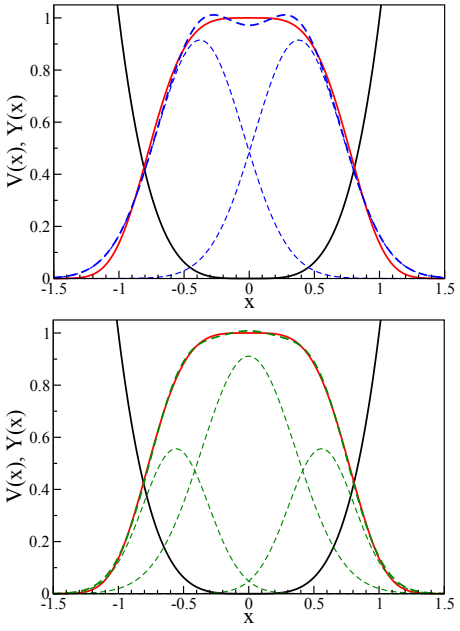

Figure 1. Quartic potential $V = x^4$ and corresponding 2-Gaussian (upper panel) and 3-Gaussian (lower panel) fits.

3.2 Double-well asymmetric potential

For $V(x) = \frac{1}{4} - x^2 + x^4$, two asymmetric wells produce a double-peaked yield at low excitation energy as shown by the solid line in Fig. 2. The 2-Gaussian fit to the yield is considerably improved by adding a third Gaussian at symmetry. However, the latter should not be interpreted as a new physical symmetric mode as it is not associated with a potential well at symmetry.

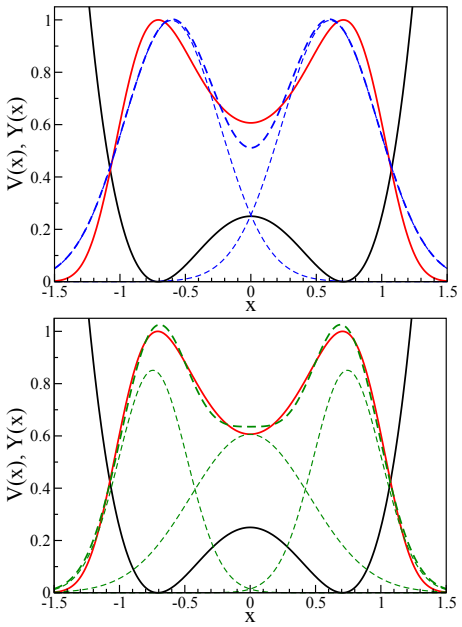

Figure 2. Yield from a two-well potential and 2-Gaussian (upper panel) and 3-Gaussian (lower panel) fits.

4 Application to experimental data

4.1 ^{180}Hg fission

Experimental mass yields from β-delayed fission of ^{180}Tl [26] and fusion-fission of ^{36}Ar+^{144}Sm [27] exhibit a transition from asymmetric to symmetric mass distributions with increasing excitation energy. These distributions are well described by two Gaussian components with stable centroids. The transition from asymmetric to symmetric fission occurs at $E^* \simeq 65$ MeV.

The reconstructed effective potentials shown in Fig. 3 evolve from a double-well to a single broad minimum as excitation energy increases, indicating a transition from shell-driven asymmetric fission to a symmetric liquid-drop regime. This approach provides a clear visual and quantitative description of the fading of shell effects. In particular, it indicates that at high excitation energy, a single effective mode is present, despite the fact that the yields could be fitted with two (strongly overlapping) Gaussian functions.

4.2 ^{238}U and ^{232}Th neutron-induced fission

Brosa *et al.* proposed the well-known Standard 1 (S1), Standard 2 (S2), and superlong symmetric modes, each

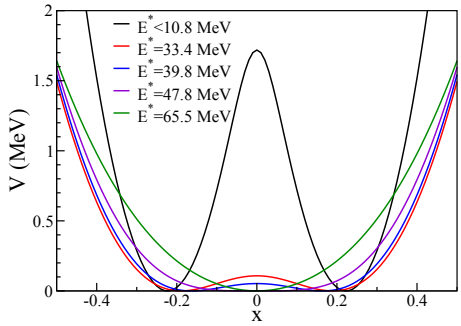

Figure 3. Effective potentials for ^{180}Hg at various E^* values. The transition from asymmetric to symmetric fission is evident.

with characteristic fragment mass and total kinetic energy (TKE) distributions [28]. Neutron-induced fission data for ^{232}Th and ^{238}U have been fitted with S1, S2, and superlong Gaussian modes [29]. The results of the fits are shown in Fig. 4.

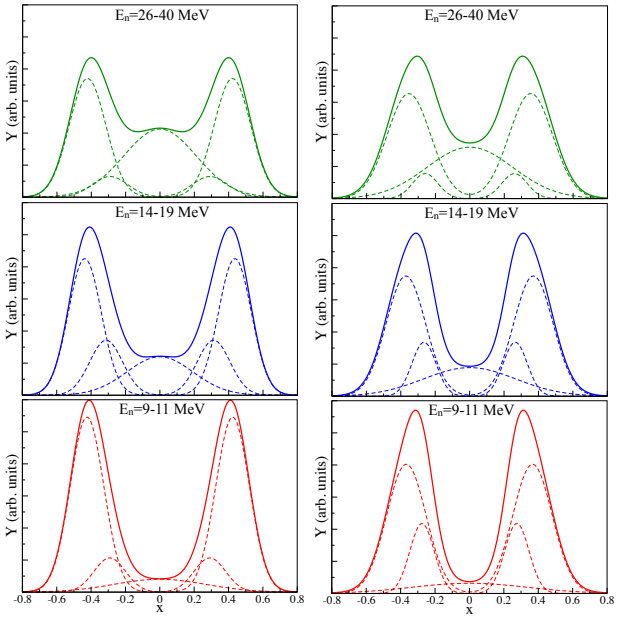

Figure 4. Gaussian fits of ^{232}Th (left) and ^{238}U (right) neutron-induced fission fragment mass distributions at various energies [29].

Associated analysis using effective potentials are shown in Fig. 5, highlighting evolution of shell effects and onset of symmetric modes. At low E^*, the effective potential exhibits a pronounced two-well structure reflecting strong shell effects in the heavy fragment induced by octupole deformed shell effects at $Z \approx 52$–56 [7]. With increasing E^*, the central barrier decreases, consistent with a reduction in shell stabilization. In ^{232}Th, an additional shallow minimum appears at symmetry, indicating the onset of symmetric fission pathways.

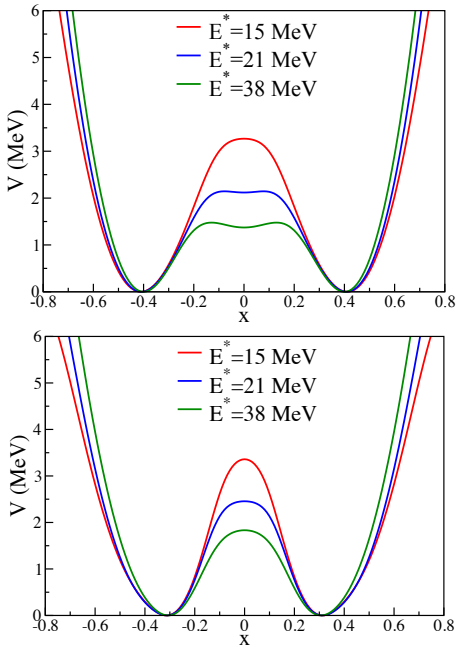

Figure 5. Effective potentials for ^{232}Th (upper panel) and ^{238}U (lower panel) extracted from the yields of Fig. 4.

5 Discussion and conclusion

The comparison between Gaussian, theoretical, and effective modes reveals several key insights [22]:

- Gaussian centroids can shift with excitation energy without implying new fission modes; such shifts often reflect the temperature dependence of the yield rather than a change in the PES.
- The effective potential provides a more direct representation of the energy landscape near scission and can distinguish genuine structural transitions (e.g., asymmetric-to-symmetric) from fitting artefacts.
- In actinides, S1 and S2 Gaussian modes merge into a single asymmetric effective mode, supporting the view that both originate from the same nonharmonic valley influenced by octupole-deformed shell gaps.
- For sub-lead nuclei like ^{180}Hg, the vanishing of the double-well structure at high E^* indicates the quenching of shell effects and the dominance of macroscopic surface and Coulomb energies.

Gaussian fits have long been employed to parameterize fission fragment distributions and identify the role of shell effects. However, this study shows that Gaussian components are not necessarily equivalent to distinct physical fission modes. By extracting effective potentials from yields, one can reconstruct the shape of the PES near scission, revealing true mode characteristics and their evolution with excitation energy.

The proposed method offers a computationally simple yet physically meaningful approach to bridge experiments and theory. When combined with microscopic models such as TDGCM, it can help constrain PES topographies

and improve our understanding of shell quenching and fission mode coexistence.

References

[1] E. Prasad, D.J. Hinde, M. Dasgupta, D.Y. Jeung, A.C. Berriman, B.M.A. Swinton-Bland, C. Simenel, E.C. Simpson, R. Bernard, E. Williams et al., Systematics of the mass-asymmetric fission of excited nuclei from ^{176}Os to ^{206}Pb, Phys. Lett. B **811**, 135941 (2020). 10.1016/j.physletb.2020.135941

[2] B.M.A. Swinton-Bland, M.A. Stoyer, A.C. Berriman, D.J. Hinde, C. Simenel, J. Buete, T. Tanaka, K. Banerjee, L.T. Bezzina, I.P. Carter et al., Mass-asymmetric fission of ^{205,207,209}Bi at energies close to the fission barrier using proton bombardment of ^{204,206,208}Pb, Phys. Rev. C **102**, 054611 (2020). 10.1103/PhysRevC.102.054611

[3] K. Banerjee, D.J. Hinde, M. Dasgupta, J. Sadhukhan, E.C. Simpson, D.Y. Jeung, C. Simenel, B.M.A. Swinton-Bland, E. Williams, L.T. Bezzina et al., Sensitive search for near-symmetric and super-asymmetric fusion-fission of the superheavy element Flerovium (Z=114), Phys. Lett. B **820**, 136601 (2021). 10.1016/j.physletb.2021.136601

[4] Bernard, R. N., Simenel, C., Blanchon, G., Hartree-Fock-Bogoliubov study of quantum shell effects on the path to fission in ^{180}Hg, ^{236}U and ^{256}Fm, Eur. Phys. J. A **59**, 51 (2023). 10.1140/epja/s10050-023-00964-2

[5] R.N. Bernard, C. Simenel, G. Blanchon, N.W.T. Lau, P. McGlynn, Fission of ^{180}Hg and ^{264}Fm: a comparative study, Eur. Phys. J. A **60**, 192 (2024). 10.1140/epja/s10050-024-01415-2

[6] B.D. Wilkins, E.P. Steinberg, R.R. Chasman, Scission-point model of nuclear-fission based on deformed-shell effects, Phys. Rev. C **14**, 1832 (1976). 10.1103/PhysRevC.14.1832

[7] G. Scamps, C. Simenel, Impact of pear-shaped fission fragments on mass-asymmetric fission in actinides, Nature **564**, 382 (2018). 10.1038/s41586-018-0780-0

[8] G. Scamps, C. Simenel, Effect of shell structure on the fission of sub–lead nuclei, Phys. Rev. C **100**, 041602(R) (2019). 10.1103/PhysRevC.100.041602

[9] K. Banerjee, D.J. Hinde, M. Dasgupta, E.C. Simpson, D.Y. Jeung, C. Simenel, B.M.A. Swinton-Bland, E. Williams, I.P. Carter, K.J. Cook et al., Mechanisms Suppressing Superheavy Element Yields in Cold Fusion Reactions, Phys. Rev. Lett. **122**, 232503 (2019). 10.1103/PhysRevLett.122.232503

[10] H.M. Albers, J. Khuyagbaatar, D.J. Hinde, I.P. Carter, K.J. Cook, M. Dasgupta, C. Düllmann, K. Eberhardt, D.Y. Jeung, S. Kalkal et al., Zeptosecond contact times for element Z = 120 synthesis, Phys. Lett. B **808**, 135626 (2020). 10.1016/j.physletb.2020.135626

[11] T. Tanaka, D.J. Hinde, M. Dasgupta, E. Williams, K. Vo-Phuoc, C. Simenel, E.C. Simpson, D.Y. Jeung, I.P. Carter, K.J. Cook et al., Mass Equilibration and Fluctuations in the Angular Momentum Dependent Dynamics of Heavy Element Synthesis Reactions, Phys. Rev. Lett. **127**, 222501 (2021). 10.1103/PhysRevLett.127.222501

[12] V.E. Oberacker, A.S. Umar, C. Simenel, Dissipative dynamics in quasifission, Phys. Rev. C **90**, 054605 (2014). 10.1103/PhysRevC.90.054605

[13] A.S. Umar, V.E. Oberacker, C. Simenel, Fusion and quasifission dynamics in the reactions ^{48}Ca + ^{249}Bk and ^{50}Ti + ^{249}Bk using a time-dependent Hartree-Fock approach, Phys. Rev. C **94**, 024605 (2016). 10.1103/PhysRevC.94.024605

[14] M. Morjean, D.J. Hinde, C. Simenel, D.Y. Jeung, M. Airiau, K.J. Cook, M. Dasgupta, A. Drouart, D. Jacquet, S. Kalkal et al., Evidence for the Role of Proton Shell Closure in Quasifission Reactions from X–Ray Fluorescence of Mass–Identified Fragments, Phys. Rev. Lett. **119**, 222502 (2017). 10.1103/PhysRevLett.119.222502

[15] K. Godbey, A.S. Umar, C. Simenel, Deformed shell effects in ^{48}Ca + ^{249}Bk quasifission fragments, Phys. Rev. C **100**, 024610 (2019). 10.1103/PhysRevC.100.024610

[16] C. Simenel, P. McGlynn, A.S. Umar, K. Godbey, Comparison of fission and quasi-fission modes, Phys. Lett. B **822**, 136648 (2021). 10.1016/j.physletb.2021.136648

[17] I. Lee, P. Stevenson, A. Diaz-Torres, Quantum mechanical treatment of nuclear friction in coupled-channels heavy-ion fusion, Phys. Lett. B **854**, 138755 (2024). 10.1016/j.physletb.2024.138755

[18] P. McGlynn, C. Simenel, Time-dependent Hartree-Fock study of quasifission trajectories in reactions forming ^{294}Og, Phys. Rev. C **107**, 054614 (2023). 10.1103/PhysRevC.107.054614

[19] C. Simenel, A. Umar, K. Godbey, P. Mcglynn, Shell effects in quasi-fission for calcium induced reactions forming thorium isotopes, Phys. Lett. B p. 139955 (2025). https://doi.org/10.1016/j.physletb.2025.139955

[20] C. Simenel, Nuclear Quantum Many-Body Dynamics: From Collective Vibrations to Heavy-Ion Collisions (2nd edition), arXiv:2506.04261 (2025).

[21] D.J. Hinde, D.Y. Jeung, E. Prasad, A. Wakhle, M. Dasgupta, M. Evers, D.H. Luong, R. du Rietz, C. Simenel, E.C. Simpson et al., Sub–barrier quasifission in heavy element formation reactions with deformed actinide target nuclei, Phys. Rev. C **97**, 024616 (2018). 10.1103/PhysRevC.97.024616

[22] P. McGlynn, C. Simenel, Extraction of fission mode properties from fragment mass distributions, Phys. Rev. C **111**, 034619 (2025). 10.1103/PhysRevC.111.034619

[23] H. Goutte, J.F. Berger, P. Casoli, D. Gogny, Microscopic approach of fission dynamics applied to fragment kinetic energy and mass distributions in ^{238}U, Phys. Rev. C **71**, 024316 (2005). 10.1103/PhysRevC.71.024316

[24] N. Schunck, L.M. Robledo, Microscopic theory of nuclear fission: a review, Rep. Prog. Phys. **79**, 116301 (2016). 10.1088/0034-4885/79/11/116301

[25] N.W.T. Lau, R.N. Bernard, C. Simenel, Smoothing of one- and two-dimensional discontinuities in potential energy surfaces, Phys. Rev. C **105**, 034617 (2022). 10.1103/PhysRevC.105.034617

[26] A.N. Andreyev, J. Elseviers, M. Huyse, P. Van Duppen, S. Antalic, A. Barzakh, N. Bree, T.E. Cocolios, V.F. Comas, J. Diriken et al., New Type of Asymmetric Fission in Proton-Rich Nuclei, Phys. Rev. Lett. **105**, 252502 (2010). 10.1103/PhysRevLett.105.252502

[27] K. Nishio, A.N. Andreyev, R. Chapman, X. Derkx, C.E. Düllmann, L. Ghys, F.P. Heßberger, K. Hirose, H. Ikezoe, J. Khuyagbaatar et al., Excitation energy dependence of fragment-mass distributions from fission of ^{180,190}Hg formed in fusion reactions of ^{36}Ar + ^{144,154}Sm, Phys. Lett. B **748**, 89 (2015). 10.1016/j.physletb.2015.06.068

[28] U. Brosa, S. Grossmann, A. Müller, Nuclear scission, Phys. Rep. **197**, 167 (1990). 10.1016/0370-1573(90)90114-H

[29] V.D. Simutkin, S. Pomp, J. Blomgren, M. Österlund, R. Bevilacqua, P. Andersson, I.V. Ryzhov, G.A. Tutin, S.G. Yavshits, L.A. Vaishnene et al., Experimental Neutron-induced Fission Fragment Mass Yields of ^{232}Th and ^{238}U at Energies from 10 to 33 MeV, Nuclear Data Sheets **119**, 331 (2014). 10.1016/j.nds.2014.08.091

[30] C. Simenel, A.S. Umar, K. Godbey, M. Dasgupta, D.J. Hinde, How the Pauli exclusion principle affects fusion of atomic nuclei, Phys. Rev. C **95**, 031601(R) (2017). 10.1103/PhysRevC.95.031601

[31] C. Simenel, P. Chomaz, G. de France, Quantum Calculation of the Dipole Excitation in Fusion Reactions, Phys. Rev. Lett. **86**, 2971 (2001). 10.1103/PhysRevLett.86.2971

[32] K. Godbey, A.S. Umar, C. Simenel, Dependence of fusion on isospin dynamics, Phys. Rev. C **95**, 011601(R) (2017). 10.1103/PhysRevC.95.011601

[33] A.S. Umar, C. Simenel, W. Ye, Transport properties of isospin asymmetric nuclear matter using the time-dependent Hartree–Fock method, Phys. Rev. C **96**, 024625 (2017). 10.1103/PhysRevC.96.024625

[34] K. Godbey, C. Simenel, A.S. Umar, Microscopic predictions for the production of neutron-rich nuclei in the reaction ^{176}Yb+^{176}Yb, Phys. Rev. C **101**, 034602 (2020). 10.1103/PhysRevC.101.034602

[35] A.S. Umar, C. Simenel, K. Godbey, Pauli energy contribution to the nucleus-nucleus interaction, Phys. Rev. C **104**, 034619 (2021). 10.1103/PhysRevC.104.034619

[36] K. Godbey, A.S. Umar, C. Simenel, Theoretical uncertainty quantification for heavy-ion fusion, Phys. Rev. C **106**, L051602 (2022). 10.1103/PhysRevC.106.L051602